Sensitivity, Hazard, and Vulnerability of Farmlands to Saltwater Intrusion in Low-Lying Coastal Areas of Venice, Italy

Luigi Tosi [1,*], **Cristina Da Lio** [1], **Alessandro Bergamasco** [2], **Marta Cosma** [1], **Chiara Cavallina** [1], **Andrea Fasson** [1], **Andrea Viezzoli** [3], **Luca Zaggia** [1] **and Sandra Donnici** [1]

[1] Institute of Geosciences and Earth Resources, National Research Council, 30131 Padova, Italy; cristina.dalio@igg.cnr.it (C.D.L.); marta.cosma@igg.cnr.it (M.C.); chiara.cavallina@igg.cnr.it (C.C.); andrea.fasson@igg.cnr.it (A.F.); luca.zaggia@igg.cnr.it (L.Z.); sandra.donnici@igg.cnr.it (S.D.)

[2] Institute of Marine Sciences, National Research Council, 30122 Venice, Italy; alessandro.bergamasco@ismar.cnr.it

[3] Aarhus Geophysics, 56023 Pisa, Italy; andrea.viezzoli@aarhusgeo.com

[*] Correspondence: luigi.tosi@igg.cnr.it

Abstract: Saltwater intrusion is a growing threat for coastal aquifers and agricultural practices in low-lying plains. Most of the farmlands located between the margin of the Southern Venice lagoon and the Northern Po delta, Italy, lie a few meters below mean sea level and are drained by a large network of artificial channels and hydraulic infrastructures to avoid frequent flooding and allow agricultural practices. This work proposes an assessment of the vulnerability to saltwater intrusion, following a new concept of the hazard status, resulting in combining the depth of the freshwater/saltwater interface and the electrical resistivity of the shallow subsoil. The sensitivity of the farmland system was assessed by using ground elevation, distance from freshwater and saltwater sources, permeability, potential runoff, land subsidence, and sea-level rise indicators. Relative weights were assigned by a pairwise comparison following the Analytic Hierarchy Process approach. The computed vulnerability map highlights that about 30% of the farmlands is under strong and extreme conditions, 28% between marginal and moderate, and 40% under negligible conditions. Results from previous vulnerability assessments are discussed in order to explain their differences in terms of hazard status conceptualization and sensitivity characterization of farmland system.

Keywords: saltwater intrusion; salinization hazard; sensitivity indicators; farmland vulnerability

1. Introduction

Saltwater intrusion is a major concern for coastal areas, especially when they comprise low-lying plains where the drainage has shifted from naturally to mostly artificially driven [1,2]. Human interventions, such as the reclamation of ancient coastal lagoons and wetlands, as well as the exploitation of groundwater, cause the expansion of the saltwater intrusion upward and landward in the aquifer systems. Over the last decades, the effects of climate change, such as drought and sea-level rise, made the problem of salinization even worse, with serious consequences on the management of farmlands and their agricultural productivity [3]. Indeed, the salinity of the soil is addressed as a strong stress factor for plants, limiting their growth and influencing crop yields [4].

A variety of methods is used to assess the saltwater intrusion in coastal aquifers and soils, and the different approaches depend on the spatial scale of investigation and the characteristics of the environment [3,5]. Once the extent of saltwater intrusion is mapped and its driving mechanisms understood, an appropriate analysis of vulnerability of a given environment to the salinization process must be developed as a first step toward the planning of effective mitigation strategies and adaptation policies.

The concept of vulnerability in the literature is generally expressed in terms of the exposure, sensitivity, and adaptive capacity of a system to a context of climate-related

hazards [6]. However, there is a rich body of the literature on the approaches for its computation, requiring the integration of multiple quantitative and semi-quantitative data [7–9]. Index-based approaches are commonly used to assess vulnerability to saltwater intrusion [5]. An important advantage of these methods is the simplicity of the functional form of the overall vulnerability index, which combines the specific magnitude of indicators, simplifying a number of complex and interacting feedbacks to a form that is more readily understood with possibly greater utility as a management tool [10,11]. For instance, canonical [12–14] and modified forms [15–19] of the GALDIT (Groundwater, Aquifer, Level, Distance, Impact, Thickness) method are among the most commonly used to assess vulnerability of groundwater to saltwater intrusion. The original form focuses on the aquifer's characteristics and considers a number of factors (indicators) that may concur to modify the vulnerability magnitude. Specifically, it includes groundwater occurrence (aquifer type; unconfined, confined, and leaky confined), aquifer hydraulic conductivity, height of groundwater level above the sea, distance from the shore, impact of existing status of saltwater intrusion, and thickness of the aquifer. A number of GALDIT modified methods include, for instance, weight and classes optimization with statistical methods [20,21], or the addition of new parameters based on local characteristics of the case studies and data availability [16,22].

One of the main limitations of the index-based methods is the weighting and rating of indicators, which are often highly user dependent [5], so that the assignment of scores through expert judgments is hardly able to define a metric structure on the field of the variable to be 'measured' through the indicators. The Analytical Hierarchy Process (AHP) [23], implemented by pairwise comparisons among the indicators, allows us to reduce the user subjectivity [16] and obtain a measure of the internal consistency of the assigned weights. This method is widely used in many different fields, and it has also recently been applied to aquifer management [24], adaptation strategies to saltwater intrusion [25], and assessment of aquifer vulnerability to seawater intrusion [16,21]. At the southern margin of the Venice Lagoon (Figure 1), almost 200 km^2 of coastal farmlands hosts a variety of crops, such as soybean, corn, and wheat. These farmlands, which are the result of hydraulic reclamation of swamp areas performed at the beginning of the last century, presently lie below the sea level, also because of the high rates of land subsidence [26,27]. The whole area is drained by a system of pumping stations connected to a distributed network of channels and drainage ditches that collects the excess inflow keeping the water table at optimal levels for farming. Over the years, this hydro-morphological setting has led to the progressive saltwater intrusion in aquifers and soils from the sea and the nearby lagoon margin. The impact now extends up to 20 km inland from the Adriatic coast, with the contaminating plume reaching depths of several tens of meters and often affecting the cultivated land [28–30]. A local mitigation of the salinity diffusion in the unconfined aquifer is provided by freshwater flow from the network of irrigation channels and direct precipitation [31].

A first-step in mapping the vulnerability to saltwater intrusion of Venice farmlands was proposed by Da Lio et al. [29]. They adopted a modified GALDIT approach that considered the features of the farmlands strongly controlled by artificial infrastructures. Specifically, relevant environmental indicators, such as the actual status of the saline intrusion resulting from electrical conductivity data measured in wells and surficial watercourses, the elevation of the ground, and the distance from salt- and freshwater sources, were combined through an easy-to-use composite vulnerability index [29]. Despite this promising approach, a satisfactory assessment of vulnerability to saltwater intrusion is still far from being achieved.

Figure 1. Location of the study area (yellow polygon) on the coast of the Northern Adriatic Sea, Italy. Base map source: Esri, Maxar, Earthstar Geographics, USDA FSA, USGS, Aerogrid, IGN, IGP, and the GIS User Community.

This study proposes an update of the assessment of the vulnerability to saltwater intrusion previously provided by Da Lio et al. [29], on the basis of an improved concept of vulnerability and a wider dataset of environmental indicators. The adopted concept of vulnerability refers to the propension of farmland systems to be negatively affected by saltwater intrusion, due to the intrinsic sensitivity of the system, when different triggers modify the present hazard status. Intrinsic sensitivity characteristics and present hazard status are described based on relevant indicators accurately selected (i.e., freshwater–saltwater interface depth, electrical resistivity of the shallow subsoil, distance from salt- and freshwater sources, ground elevation, permeability of the shallow subsoil, potential runoff, land subsidence, and sea-level rise) and then are combined by following an index-based approach.

2. Study Area

The study area is located on the northeastern coast of Italy (45°10′ N, 12°12′ E) (Figure 1); bounded by the Adriatic Sea to the east and the Venice Lagoon to the north, it extends on a surface of approximately 200 km^2. The area is crossed by the Brenta, Bacchiglione, and Adige rivers and includes a dense network of artificial channels and drainage ditches that are currently used to manage water flow in the low-lying farmlands. Most of this territory has been exploited for agricultural and livestock breeding since the beginning of 1900s, when the pre-existing wetlands were reclaimed. Today the most common crops are soybean, corn, and wheat, but in the past, sugar beet and flax were also cultivated [32].

The shallow subsoil (i.e., about 20 m depth) includes Late Pleistocene and Holocene successions (Figure 2). The Late Pleistocene deposits consist of alluvial sand, silt, and clay deposited during the Last Glacial Maximum (LGM), when the Venetian area was a vast alluvial plain [33–36] and the sea level was 110–120 m lower than it is at present [37]. The top of the Pleistocene deposits shows evident signs of pedogenesis developed in a prolonged phase of subaerial exposure [38]. A paleosol known as Caranto marks the boundary between Pleistocene and Holocene deposits [39–41] and outlines a regional

unconformity. The Holocene deposits [33,42] show the typical wedge-shaped architecture containing transgressive and highstand sequences. The transgressive sequence is composed of a thin basal layer of lagoon/back-barrier deposits passing upward to lagoon, littoral, and shelf facies in mutual heteropic relationships. The following stratigraphic units are related to the progradation of the system during sea level highstand. They consist of fluvio-deltaic and lagoonal facies in heteropic relationships, gradually passing to littoral facies toward the coast [40,41].
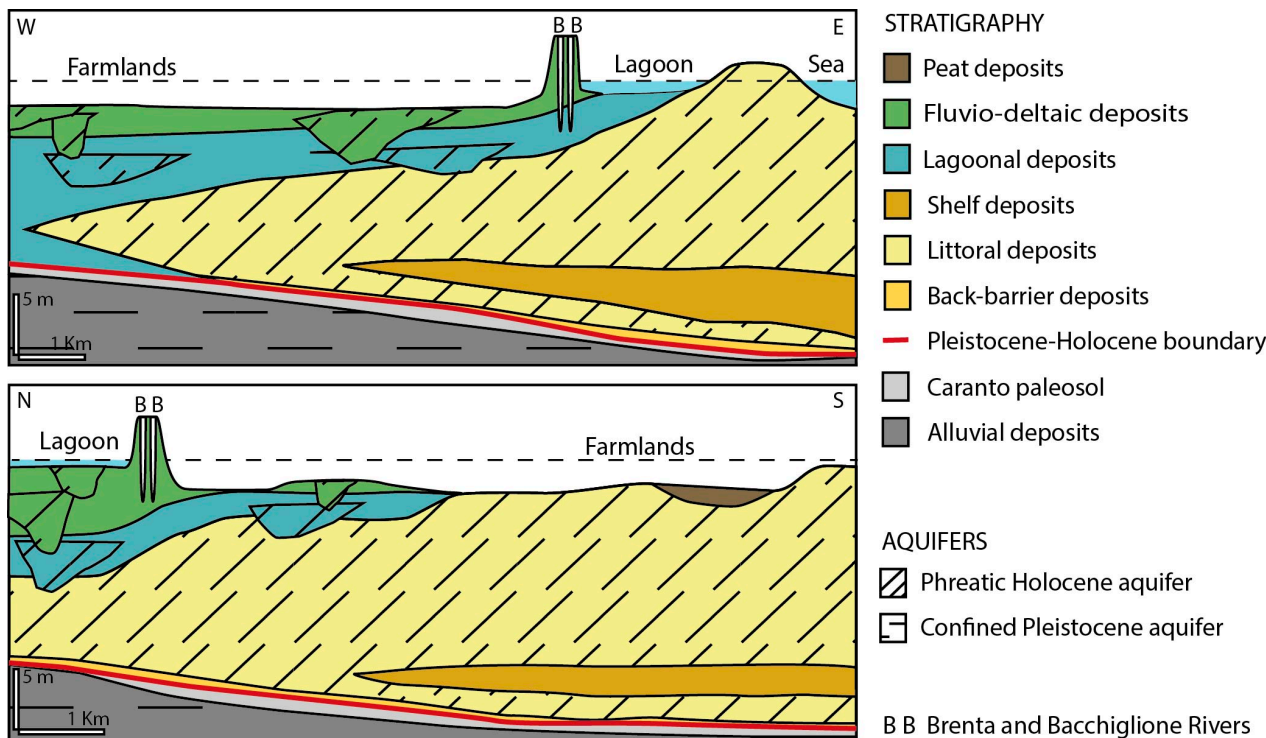
Figure 2. Schematic representation of the hydro-stratigraphic architecture of the study area.

The hydro-stratigraphic architecture is complex because of the lateral and vertical lithostratigraphic variability (Figure 2). The upper 20 m of the subsoil include (i) the phreatic aquifer, hosted in the Holocene deposits, mainly in littoral facies and channelized sedimentary bodies of fluvio-deltaic and lagoonal facies; and (ii) the Pleistocene alluvial aquifer, which is confined at the top by the Caranto layer (Figure 2). The phreatic aquifer, which is the focus of this work, locally shows a semi-confinement, due to the presence of fine-grained sediments of lagoonal and fluvio-deltaic facies.

The present-day morphology is the result of the elevation difference inherited from the low-lying swamps and the higher fluvial and coastal ridges existing before the hydraulic reclamation [43,44], which has been further exacerbated by land subsidence. Over the last 70 years, subsidence has led to a loss in ground elevation of 1.5–2.0 m [45], mainly caused by the oxidation of the organic fraction as a result of soil drainage for farming [46,47]. The present-day rate is about 1.5–2 cm/year [48]. Other types of geochemical subsidence [49], in terms of clay-layer shrinking driven by changes of saline content in the pore water, have not been investigated yet. The saline intrusion into the aquifer system and the contamination of agricultural soils progressively affected the study area, especially during the last two decades, as an effect of climate changes (e.g., droughts and sea-level rise) [29,31,50–52]. The saline plume intrudes irregularly up to 20 km inland from the nearby sea and lagoon. Its top varies from 0 to 10 m below mean sea level (MSL), whereas its bottom ranges between 15 and 70 m below MSL, and it locally deepens to 100 m [28]. The intrusion of saline waters into aquifers and agricultural soils in the sectors farthest from the sea and the lagoon edge derives from paleo-marine waters. The process is driven by the occurrence of concomitant

factors, such as the low-lying setting of the area, the drainage network connected with tens of pumping stations, and the effects of climate changes. In addition, the presence of several buried paleochannels acting as preferential pathways for groundwater flow and solute transport, together with the seawater encroachment along the river estuaries, exacerbate the salinization of farmlands [44]. The resulting depth of the freshwater–saltwater interface often rises to the agricultural soil, damaging crops. Salinity stress can inhibit the growth of corn and soybean crops [4,53], especially during prolonged drought periods.

3. Materials and Methods

This study assumes that the farmland system vulnerable to the saltwater intrusion is the subsoil, including the agricultural zone and the underneath layers up to 3–4 m depth.

The vulnerability of farmlands to saltwater intrusion is characterized by combining the modeling of the present hazard status with a suite of relevant indicators potentially concurring to modify the magnitude of the overall vulnerability. All data used in this work were already available from previous published studies and websites. Dataset, methods, indicators, and data sources used in the vulnerability assessment are summarized in Table 1.

Table 1. Sensitivity/hazard status indicators and available dataset used in the vulnerability assessment.

	Indicators	Dataset	Method	Data Source
Hazard status	Saline interface depth (SIN)	Electrical resistivity	Airborne Electromagnetic	Tosi et al. [30]
	Electrical resistivity of the uppermost subsoil layer (AER)			
Sensitivity	Distance from saltwater (SAD) and freshwater sources (FRD)	Spatial information	Satellite images	Google Earth, accessed on 31 October 2021
	Ground elevation (GEL)	Digital Terrain Model	Lidar	Regione del Veneto *
	Permeability of the shallow aquifer (PER)	Permeability of the shallow subsoil	Agriculture and pedology	ARPAV **
		Geomorphological map	Geology, Sedimentology, Geomorphology	Città Metropolitana di Venezia ***
	Potential runoff (ROF)	Hydrologic Soil Groups	Agriculture and pedology	ARPAV ****
	Relative ground level change (RGLC)	Ground displacements	SAR interferometry	Tosi et al. [54]
		Sea-level time series	Tide gauge time series	Zanchettin et al. [55]

Note: * https://idt2.regione.veneto.it/, accessed on 31 October 2021. ** http://geomap.arpa.veneto.it/layers/geonode%3Apermsuoli50k, accessed on 31 October 2021. *** https://documentidifesasuolo.cittametropolitana.ve.it/area/eventi-pubblicazioni/pubblicazioni/, accessed on 31 October 2021. **** http://geomap.arpa.veneto.it/layers/geonode%3Aidrosuoli50k, accessed on 31 October 2021.

The indicators retrieved from analyzing the datasets and the modeling approach are described in the following subsections.

3.1. Saline Interface Depth and Electrical Resistivity

The electrical resistivity of the subsoil, as an indirect measurement of salinity, represents the present status of saltwater intrusion and can be considered a proxy of the integrated contributions given by natural processes and human activities. The electrical resistivity data were acquired by using an Airborne Electromagnetic (AEM) SkyTEM system [30]. The dataset consists of about 150 km–long electrical resistivity sections acquired along north–south and west–east profiles, crossing farmlands and watercourses in a continuous and quasi-simultaneous acquisition. The collected data were processed by using the Spatially Constrained Inversion (SCI) technique [51], and the AEM outcomes were interpreted based on groundwater measurements and hydro-stratigraphic information [28,41,50,56,57].

Electrical resistivity of 10 Ωm was assumed as the limit between saline/not saline subsoils, and the saline interface depth (SIN) is defined as the shallowest transition between freshwater and saltwater. The average electrical resistivity (AER) detected in the 1.5 m–thick layer of subsoil below the ground level (GL) (i.e., the agricultural zone) is used to describe the current status of saltwater intrusion in the farmlands.

3.2. Distance from Salt- and Freshwater Sources

The water leakages from surface water bodies into the aquifer can alternate between fresh or saline, depending on the penetration of salt wedge in the estuaries during high tides and on the stream discharge. The bottom of the main watercourses lies a few meters higher than the ground elevation of surrounding farmlands; thus, it locally recharges the unconfined aquifer, according to the permeability of the subsoil. Therefore, stretches of rivers closer to the sea affected by tidal encroachment in typical summer climatic conditions were assumed as a source of saline water. On the other hand, sources of freshwater have been attributed to the remaining upstream stretches. The distance from the Adriatic Sea and the Venice Lagoon is considered in terms of surficial infiltration of saltwater caused by storm surges. The distance of the farmlands from saltwater (SAD) and freshwater (FRD) sources was obtained digitizing the path of the Brenta, Bacchiglione, and Adige rivers, together with the Cuori, Valle, and Gorzone channels from satellite imagery.

3.3. Ground Elevation

As most of the study area lies below the sea level, it would be flooded by seawater without the aid of pumping stations, which maintain the water table below the ground surface controlling the farmland drainage. Therefore, the ground surface (GEL) is closely linked to the saltwater intrusion.

Land-surface-elevation data were obtained by the Digital Terrain Model (DTM), retrieved through LIDAR (Laser Imaging Detection and Ranging) survey and made available at 5 m resolution by the Regional Government (Regione del Veneto; https://idt2.regione.veneto.it/, accessed on 31 October 2021).

3.4. Permeability of the Shallow Aquifer

The permeability indicator (PER), referred to as the first meter of the subsoil, represents the potential capability of the saline plume to migrate into the shallow subsoil. In correspondence to the buried morphological bodies, such as paleochannels and littoral ridges, this indicator was given a higher score, as these bodies act as preferential pathways for groundwater flow. The permeability data were obtained from the soil permeability map of the Veneto Region (1:50,000 scale) (http://geomap.arpa.veneto.it/layers/geonode%3Apermsuoli50k, accessed on 31 October 2021). This variable, which was identified with the saturated hydraulic conductivity (Ksat, mm/h), was estimated with pedotransfer functions (PTFs) elaborated on the basis of the soil characteristics detected in 73 soil horizons by ARPAV, 2011 [58]. The permeability in the study area varies from 0.36 mm/h (considered the lower limit of the moderately low permeability class) and more than 360 mm/h (very high) [58]. The location of paleochannels and ancient littoral ridges were extracted from the geomorphologic map of Venice (1:50,000 scale) (https://documentidifesasuolo.cittametropolitana.ve.it/area/eventi-pubblicazioni/pubblicazioni/, accessed on 31 October 2021) [59].

3.5. Potential Runoff of the Hydrologic Soil Groups

The potential runoff (ROF) was considered for identifying the sectors with different capability levels of recharging the aquifer from rainfalls: in the areas where the potential runoff is lower, freshwater from precipitation could infiltrate the shallow subsoil and mitigate the salinity. The potential runoff was obtained from The Hydrologic Soil Group by ARPAV (Regional Agency for Environmental Protection) [58], for which the method USDA NRCS 2009 was used for the definition of Hydrologic Group [60]. According to this method, each Hydrologic Group is defined on the basis of permeability (Ksat), depth

of the water level, and presence/absence of an artificial control on the water table. The Hydrologic Group layer available from http://geomap.arpa.veneto.it/layers/geonode%3Aidrosuoli50k, accessed on 31 October 2021 was simplified by obtaining three classes of ROF (low, moderately low and moderately high).

3.6. Relative Ground Level Change

The loss in elevation with respect to the mean sea level would bring the ground surface relatively closer to the freshwater–saltwater interface, increasing the vulnerability of the crops. The Relative Ground-Level Change (RGLC) consists of the combination of land subsidence and sea-level rise and was computed by using the ground-movements data reported in Tosi et al. [54], as obtained by SAR interferometry, and the rate of sea-level rise recently computed by Zanchettin et al. [55] through the analysis of tide-gauge time series. Note that, regarding land subsidence, the line-of-sight displacements detected by the satellite were assumed to be ground vertical movements to simplify the analysis for this study. This potentially introduces an error of 20–25%, which is reasonably negligible for the aim of this work (i.e., considering the class intervals adopted for the data analysis).

3.7. Modeling Approach

In order to assess the vulnerability of the coastal farmlands to saltwater intrusion, SIN and AER thematic layers, representing the present hazard status, were combined with all the intrinsic sensitivity indicators, i.e., SAD, FRD, PER, ROF, and RGLC, which potentially can alter the present status and, thus, increase the overall vulnerability (Table 1).

The modeling approach adopted in this work consists of a number of steps, as summarized in Figure 3 and described in the following:

- Relevant indicators were selected, and the corresponding dataset was gridded on a 5 m regular cell grid, using the kriging method [61], resulting in a total of 7,767,096 nodes for each thematic layer.
- Each layer was classified into five intervals of increasing importance, with respect to its contribution to sensitivity or hazard status. Maximum and minimum boundaries between classes were chosen based on previous investigations [29,30,50,51]. The intermediate limits were instead defined by analyzing the nodes frequency distribution and classifying them through an equal area criterion. In order to create homogenous ranking between different layers, a score ranging between 0 and 4 was assigned to each class, representing the increasing contribution to the vulnerability of the system.
- The sensitivity map was estimated according to the following Equation (1):

$$Sensitivity = \frac{\sum_{i=1}^{n} \omega_i I_i}{\sum_{i=1}^{n} \omega_i} \tag{1}$$

where the *n sensitivity* indicators (*I*) (i.e., SAD, FRD, PER, ROF, and RGLC) were weighted (ω) by using pairwise comparisons, following the AHP approach [23,62], a technique developed for multicriteria decision-making problems. AHP is a scaling method to be applied to prioritized indicators, where relative scales are derived by using expert judgements and given in the form of pairwise comparisons. The AHP analysis was performed by using the R-package ahpsurvey (v. 0.4.1) by Cho [63]. The AHP also provides a mathematical measure to determine the consistency of judgments. The coherence of the pair-wise comparisons is calculated to ensure the proportionality and transitivity of the results by calculating the consistency ratio (CR), as defined by Saaty 1990 [23], who also suggests that the CR of the order of 0.1 or less is considered to be a reasonable level of consistency [23].

- The vulnerability map was then computed by combining the sensitivity map with the present hazard status, following Equation (2):

$$Vulnerability = Sensitivity + Hazard\ status \tag{2}$$

Three different hazard statuses were considered: (i) SIN; (ii) AER; and (iii) their combination, i.e., SIN&AER.
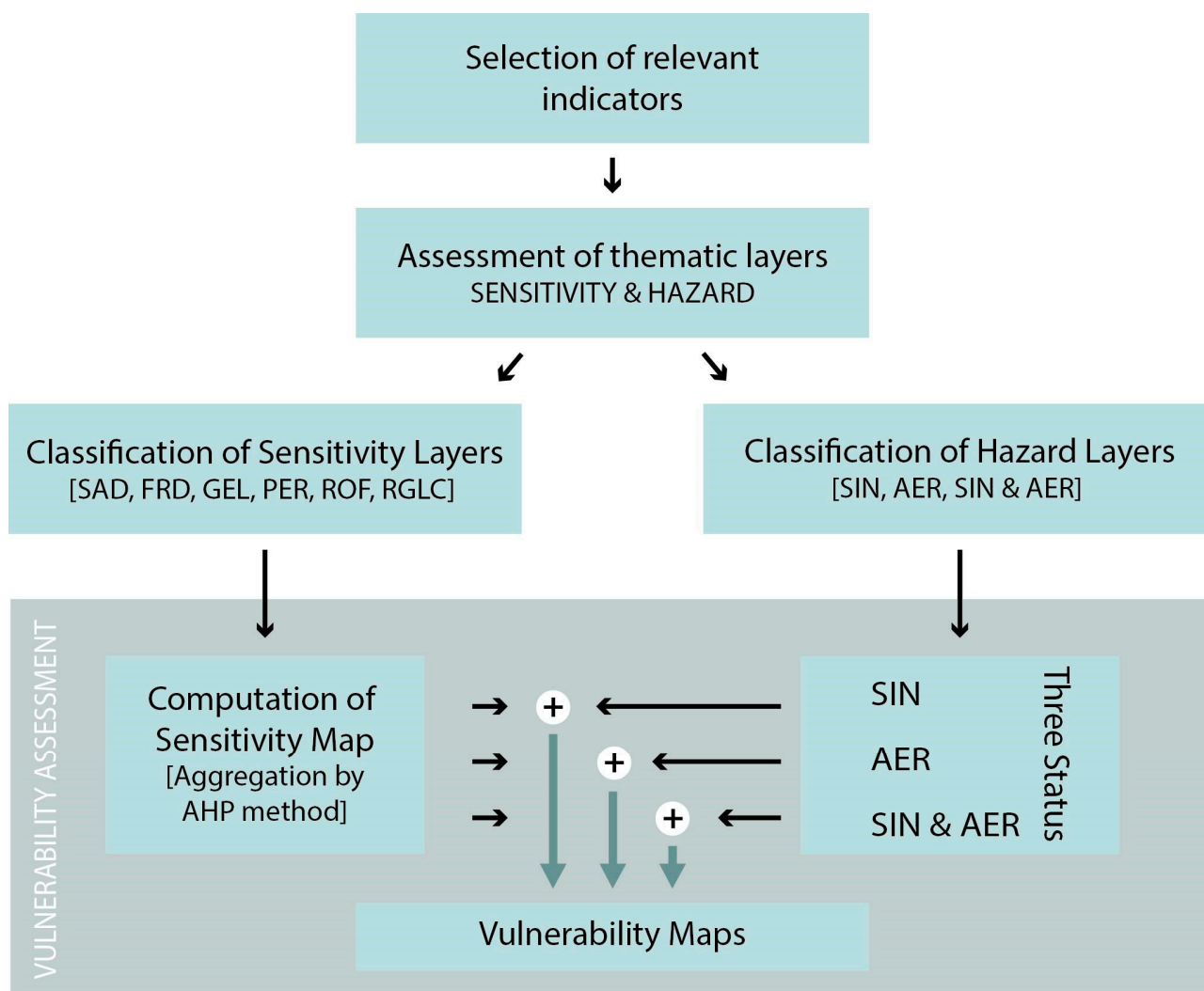
**Figure 3.** Workflow of the approach adopted to compute vulnerability maps.

4. Results

Each thematic layer was categorized into five classes with respect to its contribution to vulnerability, with progressively increasing importance. In order to determine the boundaries between classes, two criteria were used to define the extreme and intermediate values, respectively. Limits were chosen based on the experience of previous investigation and by analyzing the statistical distribution of the data.

4.1. Sensitivity Layer Classification

The classification of salt- and freshwater distance thematic layers (SAD and FRD) was based on the expected effect of salinization/freshening of the subsoil by the nearby watercourses, as observed through the monitoring well networks and in the AEM data [29,30,50]. Overall, salt- and freshwater dispersion significantly decreases within some hundreds of meters from the source. The classification of distance adopted for saline watercourses was applied also to seashore and lagoon margins affected by surficial infiltration of saltwater due to storm surges. The minimum and maximum distances considered in the classification of SAD and FRD are 100 and 800 m (Figure 4).
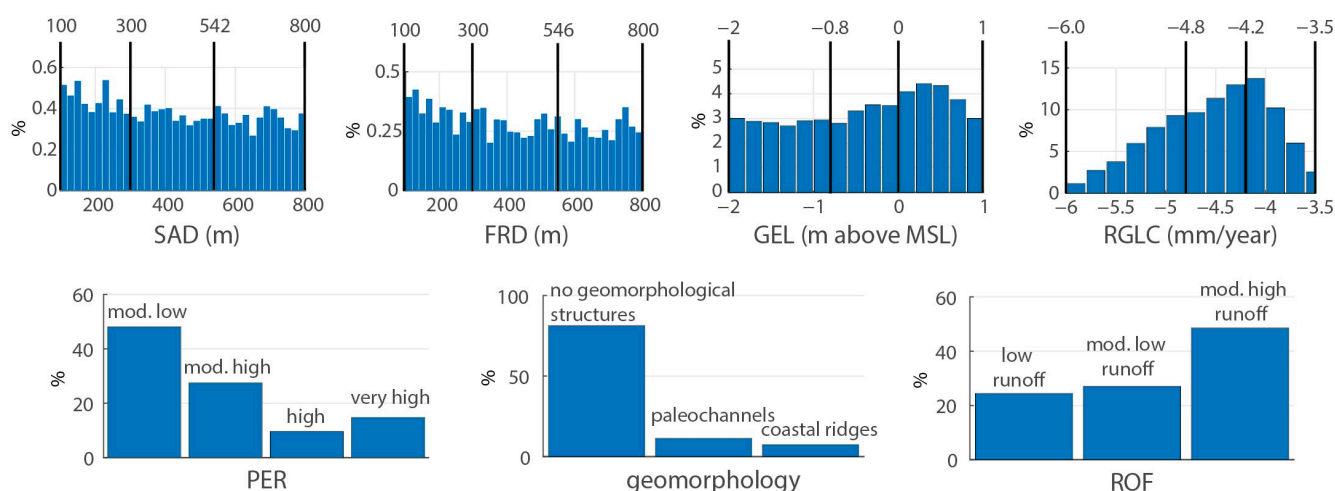
Figure 4. Frequency distribution of each sensitivity layer in the dataset (i.e., percentage of nodes in each thematic layer class over the total amount of nodes considered in the study area) confined within the minimum and the maximum boundaries set for scores 0 and 4, respectively. The abbreviation mod. means moderately, the acronym MSL stands for mean sea level.

The ground elevation level is considered to highly influence salinization processes, since a large part of the study area lies below the mean sea level, and without the artificial management of the water table, most of the coastland would be naturally flooded by the sea. Locally, freshwater lenses could develop in the surficial aquifer where the ground elevation is above the mean sea level (e.g., in the littoral sector). Therefore, areas with ground level higher than 1 m above MSL were assumed to be negligibly sensitive to the salinization process, while those lying below −2 m were given the highest importance.

The classification of the permeability and potential runoff layers was primarily based on the original classification [58]. Considering that geomorphological structures, such as paleochannels and coastal ridges, act as preferential pathways for saltwater intrusion, we combined the information obtained from the geomorphological map with the PER layer. In particular, each PER class was increased by one (e.g., class 1 was raised to class 2) wherever a buried permeable sedimentary body occurred. Overall, about 19% of the study area changed to a worse class due to this effect (Figure 4).
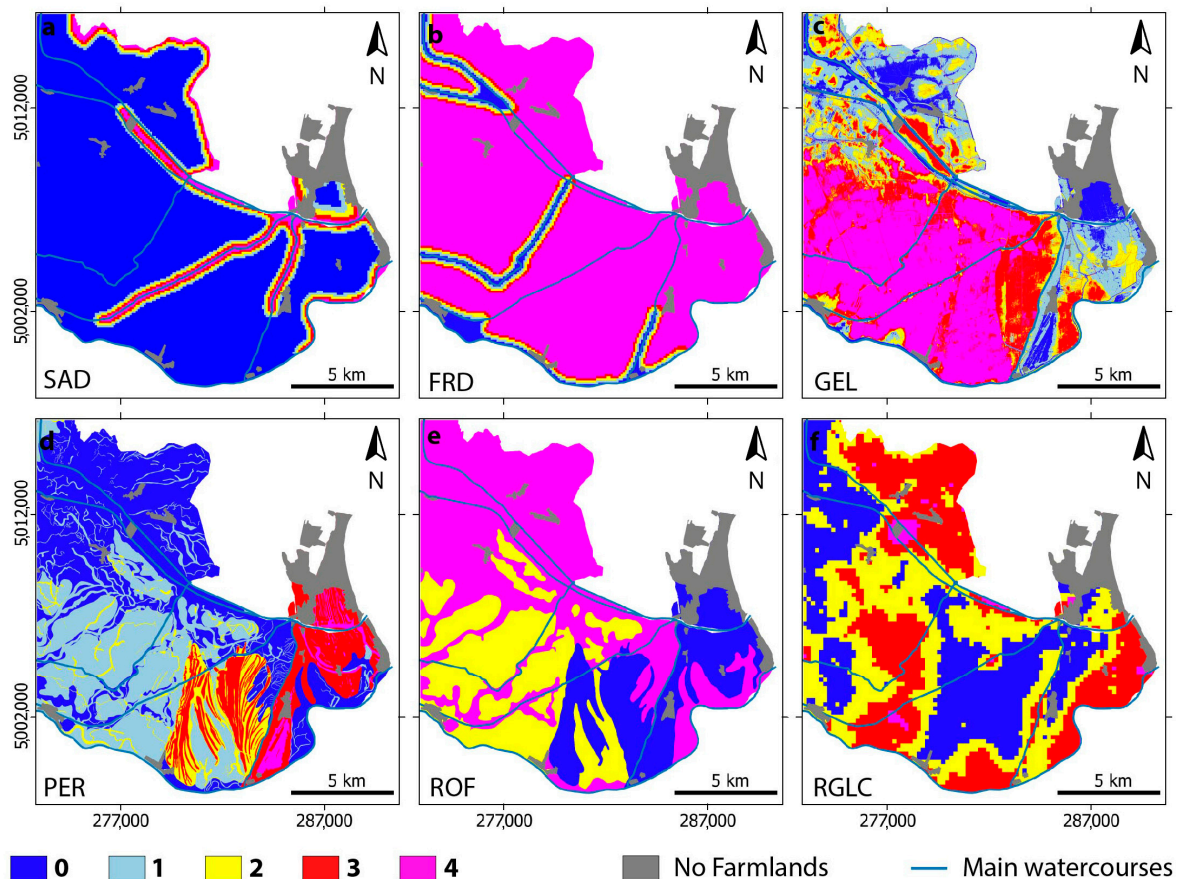
For the classification of the relative ground-level change, which results from the land subsidence increasing from the sea-level rise, the values of −3.5 and −6 mm/year were used for defining the lowest and highest classes of importance, respectively. Within this range, about 97% of the study area is included (Figure 4).

The intermediate limits, as classified through an equal area criterion of the nodes distribution, are shown in Table 2, which reports the ranges and scores of the thematic layer classification (Figure 4).

Table 2. Sensitivity-layer classification: ranges and scores. The values of 0 and 4 represent low and high contribution to vulnerability, respectively. Note that PER ranking is increased of one score point in correspondence to geomorphological structures.

SAD m	FRD m	GEL m above MSL	PER mm/h	ROF	RGLC mm/Year	Score
>800	<100	>1	moderately low 0.36–3.6	low	>−3.5	0
546–800	100–300	0.0–1.0	moderately high 3.6–36		−4.2 to −3.5	1
300–546	300–542	−0.8 to 0.0	high 36–360	moderately low	−4.8 to −4.2	2
100–300	542–800	−2.0 to −0.8	very high >360		−6.0 to −4.8	3
<100	>800	<−2.0		moderately high	<−6.0	4

Once the sensitivity layers were classified, a score from 0 to 4 was assigned, going from low to high contribution to vulnerability, in accordance with several methods available in the literature [16,22,64]. Figure 5 shows the results of the classification of each thematic layer in the study area, with color-coding highlighting the rating in accordance with the classification shown in Table 2.

Figure 5. Classification of the sensitivity layers: (**a**) saltwater distance (SAD), (**b**) freshwater distance (FRD), (**c**) ground elevation level (GEL), (**d**) permeability (PER), (**e**) potential runoff (ROF), and (**f**) relative ground-level change (RGLC). Scores from 0 to 4 identify low-to-high contributions to vulnerability. Note that PER layer combines permeability and geomorphological structures. Coordinate system: UTM33, WGS84.

4.2. Hazard-Layer Classification

The present status of the salinity hazard is described by the magnitude of the salinization process in relation to the farmland systems. The magnitude was retrieved by the AEM, survey reaching almost 100 m depth below the ground level in terms of electrical resistivity sections, here used as an indirect measurement of the subsoil salinity. Therefore, the two indicators obtained by AEM dataset, i.e., the depth of the freshwater–saltwater interface and the average electrical resistivity of the shallow subsoil, were selected to describe the actual salinization state of the farmland systems.

The hazard layers (i.e., SIN; AER; and their combination, i.e., SIN&AER) were categorized into five classes with respect to their contribution to vulnerability, with progressively increasing importance, following the same criteria adopted for the classification of the sensitivity layers.

For the saline interface depth, the highest level of hazard is assumed to be at a depth lower than 1.5 m, in order to account for the seasonal variations of the water table induced by hydraulic regulations. The lowest level of hazard was defined at a depth of 6 m below ground, reasonably assumed as the maximum depth where land-reclamation activities and climate changes have acted, at least over a decade.

Maximum and minimum values of the average electrical resistivity hazard of the shallow subsoil were set at values of 2 and 10 Ωm, respectively. In fact, based on monitoring wells' data [28,50], these resistivity values generally refer to a groundwater salinity of approximately 30–35 g/L and 3–5 g/L.

When considering the average electrical resistivity combined with the saline interface depth, the five AER classes were combined with only the SIN classes belonging to the depth interval 0–1.5 m, representing the agricultural zone. The frequency distribution of the nodes of the thematic layers and the thematic layer classification are shown in Figure 6 and Table 3, respectively.
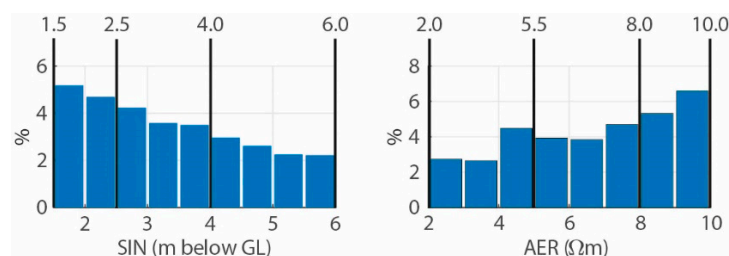

Figure 6. Frequency distribution of the dataset in each hazard layer (i.e., percentage of nodes in each thematic layer class over the total amount of nodes considered in the study area) confined within the minimum and the maximum boundaries set for score 0 and 4, respectively. The acronym GL means ground level.

Table 3. Hazard-layer classification: ranges and scores. The values of 0 and 4 mean low and high contribution to vulnerability, respectively.

SIN m below GL	AER Ωm	Score
>6.0	>10.0	0
4.0–6.0	8.0–10.0	1
2.5–4.0	5.5–8	2
1.5–2.5	2.0–5.5	3
<1.5	<2.0	4

The classified hazard layers are reported in Figure 7. The map obtained by SIN depicts a general variability of the hazard classes, with the worse conditions being in the sectors close to the lagoon margin (Figure 7a). Regarding the hazard mapped by the AER, it shows

0-score extent for the most part of the study area, and it increases to the highest, i.e., 4-score, only close to the lagoon margin (Figure 7b). The combined threat of SIN and AER highlights a general decrease hazard condition when considering high scores of SIN combined with low scores of AER in the uppermost soils (Figure 7c).
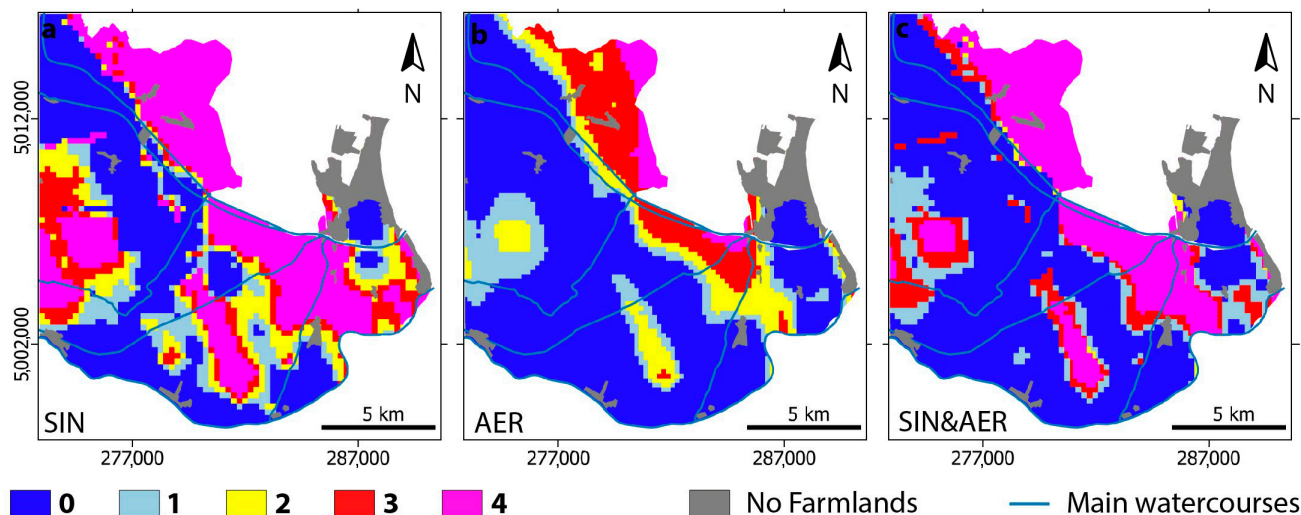
Figure 7. Classification of the hazard layers: (**a**) freshwater–saltwater interface depth (SIN), (**b**) average electrical resistivity (AER), and (**c**) freshwater–saltwater interface depth (SIN) combined with average electrical resistivity (SIN&AER). Scores from 0 to 4 identify low-to-high contributions to vulnerability. Coordinate system: UTM33, WGS84.

4.3. Sensitivity Setup of the Farmland System

The sensitivity map was obtained by combining the classified sensitivity layers according to Equation (1). The AHP process [23] was implemented through the judgments of six experts in different disciplines related to the saltwater intrusion in coastal areas (e.g., hydrogeology, stratigraphy, and oceanography) by compiling a pairwise comparison matrix for the sensitivity indicators.

The individual preference weights (green dots in Figure 8) were computed by using the Dominant Eigenvalue method described in Saaty [62] and were then aggregated by arithmetic averaging (red crosses in Figure 8). A certain degree of heterogeneity (Table 4) resulted, despite the fact that the six expert judgements were consistent, with an overall mean consistence ratio (CR) of 0.03, which is well below the suggested threshold (one case exhibiting CR = 0.1, red dots; the remaining five cases being largely <0.1).

The resulting weights (Table 4) allow us to rank the factors with respect to their expected contribution in the sensitivity computation. The weight of ground-elevation resulted in being the highest, almost double that of the relative ground-level change, whereas the other contributions are significantly lower.

The resulting sensitivity map (Figure 9) shows high heterogeneity in the distribution of the sensitivity classes, thus emphasizing the geomorphological conditions of the study area, i.e., the ground elevation and the presence of the buried sand bodies. Extreme and negligible sensitivity classes are limited in extent and generally correspond to narrow strips along the Gorzone Channel, along the Brenta and Bacchiglione rivers, and in the inner part of the coastal ridges. Sectors with marginal-to-strong sensitivity classes are almost evenly distributed and cover most of the central area.
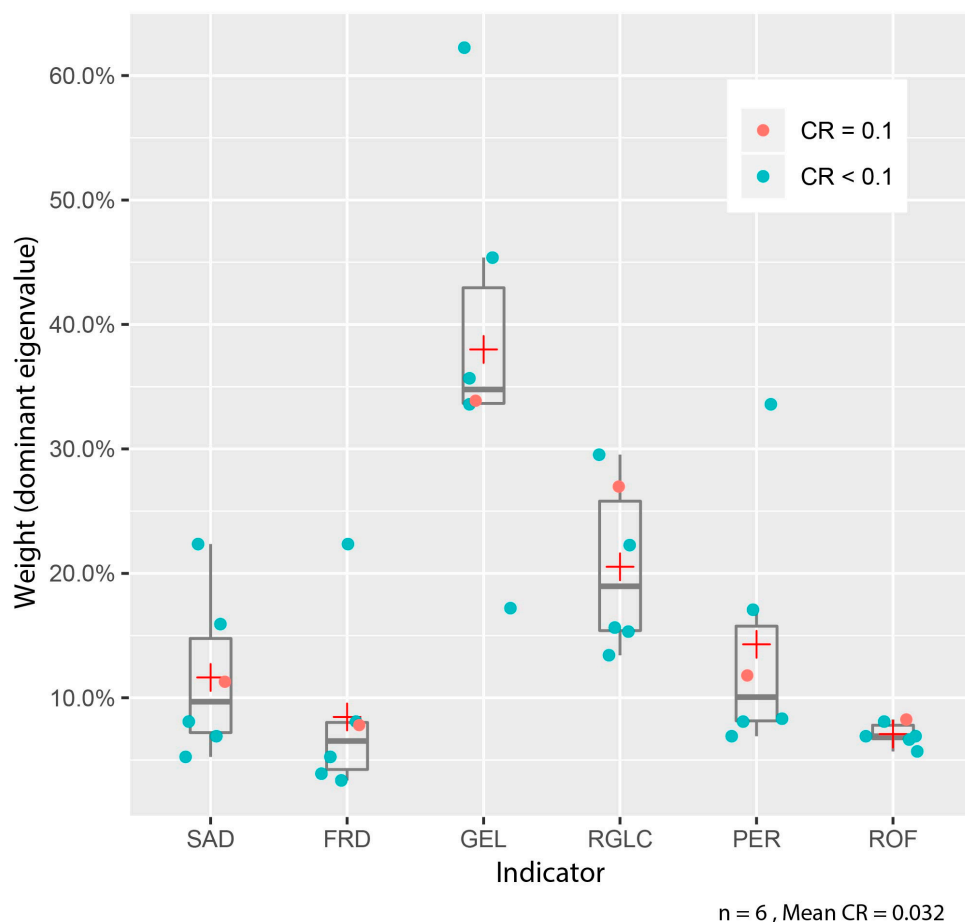
Figure 8. AHP technique application to determine the weights of the six sensitivity indicators. Red crosses indicate the mean weight computed by averaging the weights obtained from each expert.

Table 4. Weights assigned to each sensitivity indicator resulting from the AHP process: mean, standard deviation (SD), and percentage.

| Sensitivity Indicators	Weight		
	Mean	**SD**	**(%)**
SAD	0.117	0.06	11.7
FRD	0.084	0.07	8.4
GEL	0.373	0.14	37.3
RGLC	0.208	0.06	20.8
PER	0.145	0.09	14.5
ROF	0.073	0.01	7.3
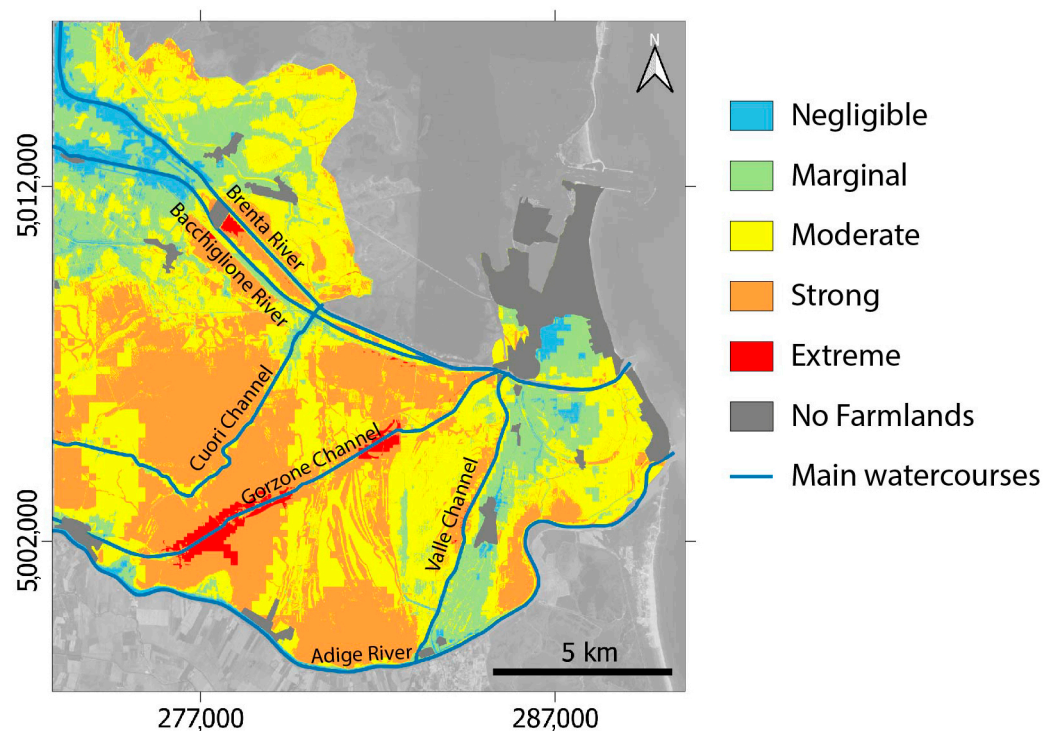
Figure 9. Map of sensitivity of farmlands to saltwater intrusion. The map was computed by accounting for the sensitivity indicators: SAD, FRD, GEL, RGLC, PER, and ROF. Coordinate system: UTM33, WGS84.

4.4. Vulnerability Analysis of the Farmland System

According to the adopted procedure, three vulnerability maps were produced (Figure 10). Vulnerabilities are described by five classes: negligible, marginal, moderate, strong, and extreme. Specifically, the vulnerability is investigated by considering three hazard statuses. The first and second statuses separately account for the indicators representing the depth of the freshwater–saltwater interface and the average electrical resistivity of the shallow subsoil. The third one combines the former status to capture the threat of the resistivity in specific sectors of the farmlands where the saline interface is at depths lower than 1.5 m below the ground.

The vulnerability map, computed by considering the SIN-hazard status, results in rather equally spatially distributed classes, covering 15% to 25% of the area (Figure 10). Conversely, in the vulnerability maps computed by considering AER- and SIN&AER-hazard statuses, the marginal (46%) and negligible (41%) classes prevail, respectively. All the vulnerability maps are clearly a signature of the considered hazard status. Interestingly, strong-to-extreme classes occur in specific areas for all the vulnerability maps. In detail, lagoon borders, the littoral at the Brenta–Bacchiglione river mouth, the seaward portion of the Adige river, and some local sectors up to 10–15 km inland exhibit the highest scores. Similarly, some areas fall into the negligible class in all the vulnerability maps, e.g., the area of Sottomarina (Figure 1), the northwestern inland between the Brenta and the Bacchiglione rivers, and the right side of the Valle channel.
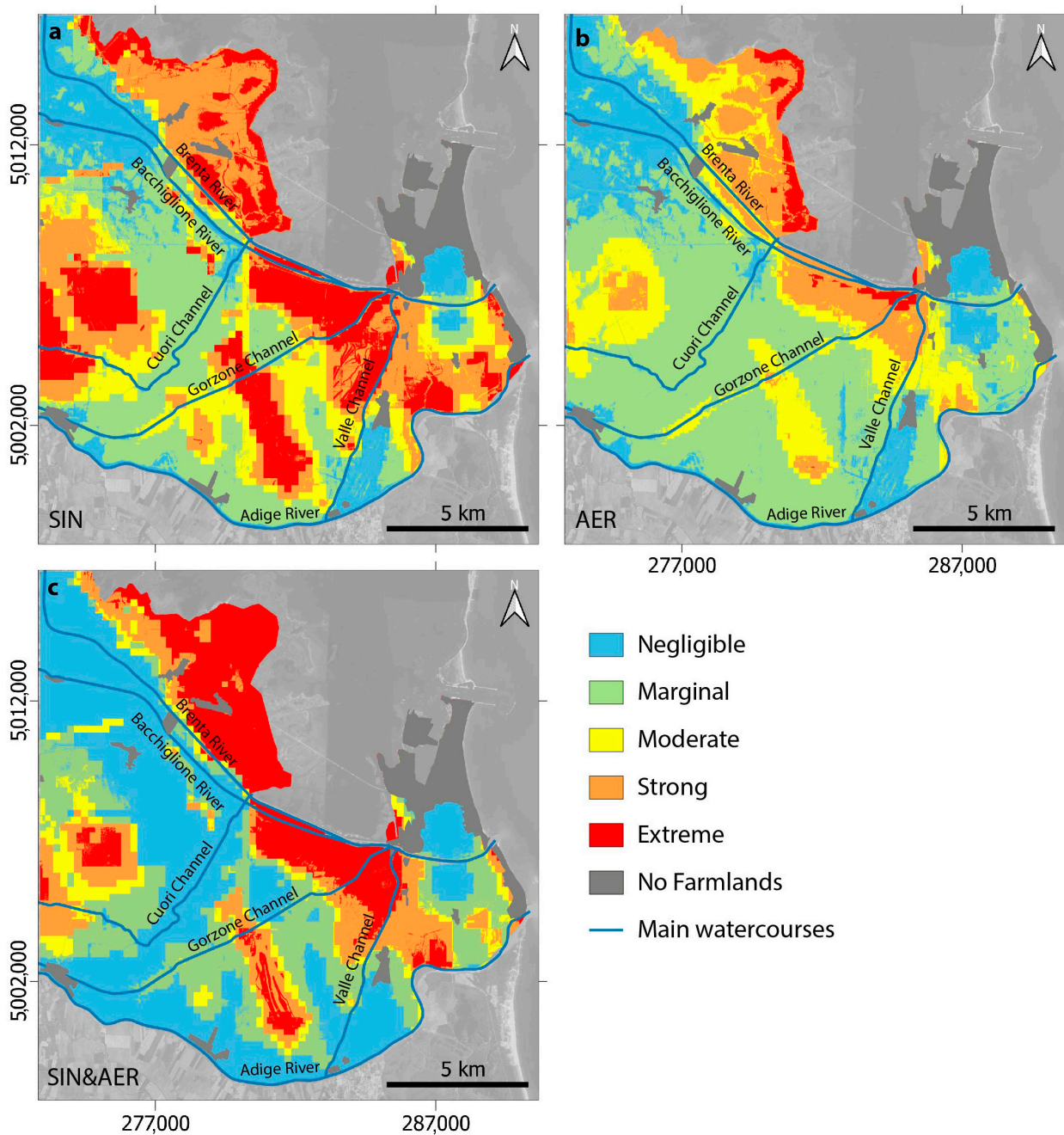
Figure 10. Maps of the vulnerability of farmlands to saltwater intrusion. The maps were computed while accounting for the sensitivity of the farmlands and the three hazard statuses: (**a**) SIN hazard, (**b**) AER hazard, and (**c**) SIN&AER hazard. Coordinate system: UTM33, WGS84.

5. Discussion

There is a wide agreement that coastal farmlands are being negatively affected by saltwater intrusion and soil salinization, which alter the quality of natural groundwater resources and reduce the overall agricultural productivity.

Over the last decades, saltwater intrusion in the Venice coastland has drawn the attention of farmers and water authorities, giving grounds for several studies aimed at understanding the mechanisms driving the salinization of aquifers and soils. The collection of a large amount of information over the last decades has significantly improved our knowledge on the mechanism driving salt intrusion [28,30,31,50–52,65]. However, it is still essential to assess the vulnerability of farmlands to saltwater intrusion, understanding

how it is generated and how it may increase, to effectively manage present and future threats. In this section, results, limits, and uncertainties of the vulnerability analysis are firstly discussed. Secondly, the outcomes of this work are compared with those reported by Da Lio et al. [29].

An important point to be considered in the analysis of the vulnerability to saltwater intrusion is the definition of the environmental target. Clearly, the vulnerability analysis of the aquifer is different from that of the farmlands. In addition, a specific model of farmland system must be conceptualized according to the boundary conditions. In this study, the farmland system that is likely vulnerable to the saltwater intrusion is assumed to be the subsoil, which includes the agricultural zone and the underneath layers up to 3–4 m depth.

Looking at the SIN and AER hazard status (Figure 7), we see that farmlands should be strongly affected by saltwater intrusion where the freshwater–saltwater interface rises close to agricultural soil and high AER values occur. However, our SIN- and AER-hazard comparison shows rather opposite conditions in some areas. For this reason, the SIN&AER was deemed to be more representative of the farmland-system hazard status than those computed by considering the indicators separately. In fact, according to our definition of farmland system, the vulnerability assessment computed by using the SIN-hazard status is likely overestimated with respect to that of AER-hazard status (Figure 10). Meanwhile, the use of the SIN&AER-hazard status permits us to adjust some classes apparently over- or underestimated by hazard status, based on SIN and AER separately. For example, the northern area bounding the lagoon margin increases in vulnerability when moving from the strong to extreme class, while the inner region behaves oppositely, and vulnerability decreases from the strong to the negligible class. Consequently, the contrast on the map is enhanced, and buffering zones of smooth transition between intermediate and extreme vulnerability are absent. SIN&AER is more coherent with AER where vulnerability is low (about 12,000 hectares); vice versa, it is more coherent with SIN where vulnerability is extreme (about 6000 hectares). This means that the remaining 10% of the study area is in the intermediate-vulnerability class.

A comparison between the three vulnerability maps is summarized in Figure 11. A rather equal spatial distribution of the vulnerability classes results by considering the SIN-hazard status, covering 15% to 25% of the area. Conversely, the marginal (46%) and negligible (41%) classes prevail when using the AER- and SIN&AER-hazard statuses.
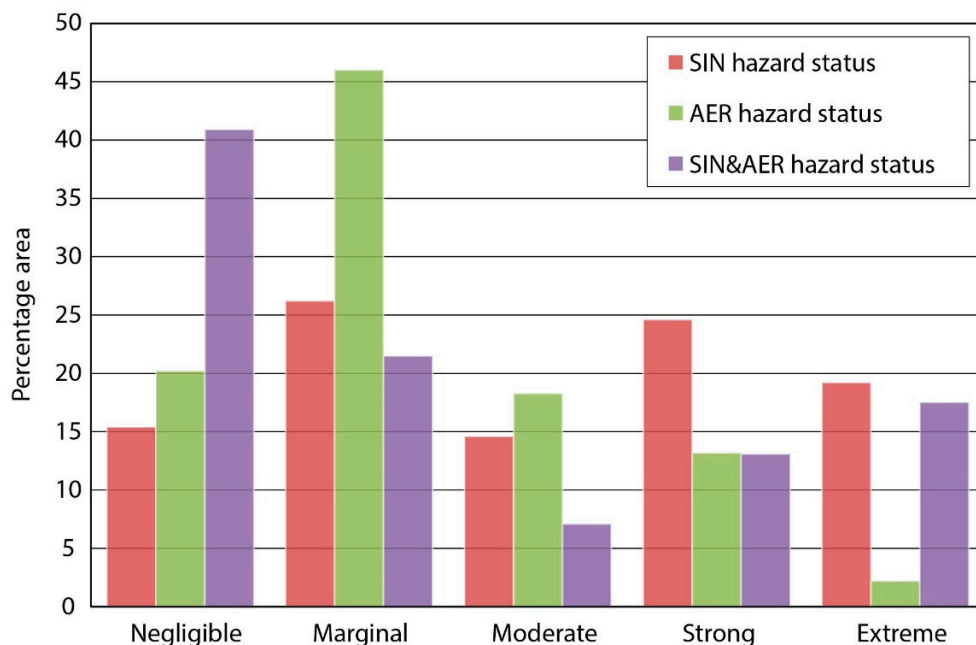

Figure 11. Areal extent of vulnerability classes (%) for the three hazard statuses.

Overall vulnerability assessments are commonly based on the proper aggregation of a selection of multiple relevant indicators, concerning sensitivity and hazard status of a system.

Beyond the intrinsic limitation of the methods of acquisition and setup of the thematic layers, the major limit of these assessments is the high degree of subjectivity. In fact, the choice of indicators relevant for the specific threat, their classification based on the importance, the aggregation procedures, and the indicator weighting are not standardized, and, thus, they are affected by subjective judgments. In this study, it should be noted that the chosen indicators are not exhaustive for a comprehensive description of the vulnerability status of the farmland system. Specifically, the variability of precipitation and details on the agricultural type covers and crop physiology are not included in this analysis. However, the use of these indicators would have required specific skills; consequently, we preferred to simplify the assessment by avoiding evaluation errors that would have increased subjectivity.

Concerning the classification, an intrinsic subjectivity is due to both the selection of minimum and maximum limits, defined based on previous knowledge, and the decision to define intermediate classes through an equal area criterion. Even though the use of the AHP approach through pairwise comparison reduced the subjectivity of expert judgments and verified their consistency, the aggregation and weighting of sensitivity/hazard indicators still maintain a degree of subjectivity. The comparison between vulnerability results obtained from different studies has to be carefully considered, because the concept of vulnerability in the literature is complex, and it is described by a variety of definitions [66,67]. Furthermore, the concept of vulnerability to saltwater intrusion in coastal plains still assumes various meanings, which are often ambiguous. In addition, over the last decades, the greater attention given to this issue has brought a significant increase in the number of case studies worldwide. This gave rise to a multitude of methodologies, which differ for the type and number of indicators chosen for the sensitivity and hazard computation. The choice of one methodology instead of another mostly depends on the availability of the indicator dataset and the specific characteristics of the study areas. Therefore, despite the use of a specific methodology and the subjective assumptions, the comparison among different research studies is often limited due to the adoption of different types of sensitivity- and hazard-status indicators. For example, Da Lio et al. [29] proposed a first assessment of the vulnerability of low-lying farmlands to saltwater intrusion in almost the same area of the present research.

The present study introduces a more detailed concept of farmlands potentially impacted by salinization and some important methodological differences with respect to the previous investigation [29]. The first main difference regards the target of the vulnerability. Indeed, Da Lio et al. [29] refers to a generic farmland concept whose assessment results in its being much more fitting to the vulnerability of the aquifer rather than the agricultural soil and the shallow subsoil. Since, in Da Lio et al. [29], the depths of the well filters are generally deeper that 4–5 m below the ground surface, electrical conductivity (EC) measurements missed the salinity status in the agricultural zone. In addition, fresh/brackish layers were neglected for piezometers filtered along the entire length, since Da Lio et al. [29] considered the worst condition of the EC values collected in the density-stratified water column. Conversely, the present study benefitted from the AER resistivity of the first 1.5 m, which provided salinity information on the subsoil layer directly in contact with crops and the upper part of the aquifer. The second difference regards the number of indicators. Only three sensitivity and one hazard indicators were used by Da Lio et al. [29], instead of the six and two, respectively, used in this work (Table 5). The third difference concerns the classes of importance related to the distance from the saline water bodies. Accounting for the results from previous investigations [31,50–52], the maximum and minimum distances adopted by Da Lio et al. [29], i.e., 500 and 4000 m, resulted in overestimating the saline impact on the farmland system. Therefore, it is reasonable to assume that the distances adopted in the present study (i.e., 100 and 800 m) better fit with those used in

Kazakis et al. [16], who assessed the aquifer vulnerability to seawater intrusion in the Po river lowlands just south of the study area. Considering the aforementioned differences and that only minor changes occurred in the salinization process during the time interval between the two studies, the present and previous assessment [29] clearly differ in some sectors (Figure 12a,b). The vulnerability map of the present study shows a general less critical situation than that provided by Da Lio et al. [29]. This is because (i) the present study successfully captures the fresh or brackish shallow subsoil (about 1–1.5 m thick) pertaining to the farmlands system that, for the reasons stated above, cannot be detected through the network of wells installed in this area; and (ii) the watercourse influence acts on shorter distances, e.g., the area adjacent of the Gorzone Channel and Brenta–Bacchiglione rivers. It should also be noted that areas not devoted to agriculture were excluded from the present study. The most obvious case is the Sottomarina sector, where the common areas analyzed by the two studies differ significantly for the reasons discussed above.

A more comprehensive comparison can be performed by considering the study area as a whole. In this case, a rather different distribution of the vulnerability classes emerges (Figure 12c). The negligible class shows the major difference, having increased by 38% compared to Da Lio et al. [29], while the moderate and strong classes decreased by about 18%. The extreme and marginal classes increased and decreased, respectively, by less than 10%, thus showing almost similar values for the two studies.

Table 5. Summary of the target and sensitivity/hazard status indicators used in this study and by Da Lio et al. [29] for the vulnerability assessment.

	Present Study	Da Lio et al. [29]
Target	A specific farmland system by referring to the subsurface layer that includes the agricultural zone and the underneath shallow subsoil up to 3–4 m depth	Generic farmlands taking into account the phreatic aquifer up to 10 m depth
Sensitivity indicators	Distance from salt- and freshwater sources (100 and 800 m are considered as likely the minimum and maximum distances influencing the sensitivity of the farmland system); Ground elevation; Permeability of the shallow aquifer; Potential runoff; Relative ground level change	Distance from salt- and freshwater sources (500 and 4000 m were considered as likely the minimum and maximum distances influencing the sensitivity of farmlands); ground elevation
Hazard indicators	Saline interface depth; electrical resistivity of the uppermost subsoil layer (1.5 m thick), which includes unsatured and satured agricultural soils	Electrical conductivity detected in wells screened at depths between 2 and 10 m below ground level or taking into account the worst condition in wells with the entire length screened where the water is density-stratified in the water column
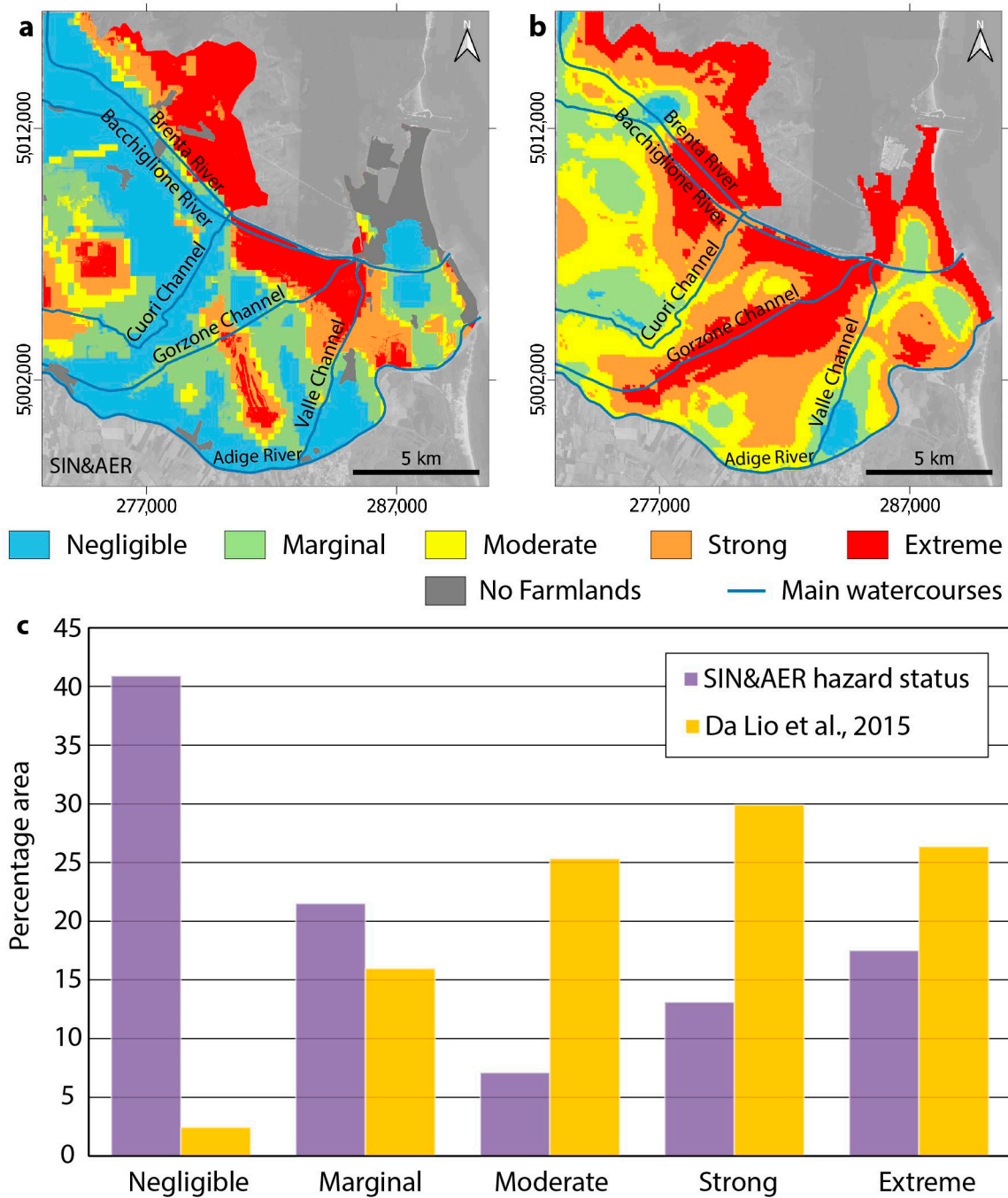
Figure 12. Maps of the vulnerability of farmlands to saltwater intrusion resulting from (**a**) this study and (**b**) Da Lio et al. [29]; (**c**) areal extent of the classes (%) for vulnerability status computed in the present study and by Da Lio et al. [29]. Coordinate system: UTM33, WGS84.

6. Conclusions

This work proposes an assessment of the vulnerability of the Venice coastland farmlands to saltwater intrusion by combining the intrinsic sensitivity characteristics with the present hazard status of salinization. The farmlands were studied by referring to a farmland system assumed as the subsurface layer that includes the agricultural zone and the underneath shallow subsoil up to 3–4 m depth, where saltwater intrusion may threaten agricultural productivity. The sensitivity to saltwater intrusion was set up by aggregating six physical indicators that potentially concur to intensify or mitigate salinization effects on the farmland system. The aggregation was computed by using pairwise comparisons

among the indicators, following the AHP approach. Regarding the salinization status, a new approach was defined for delineating the saline-hazard status on the system. The approach consisted of considering the freshwater–saltwater interface depth and the average electrical resistivity of the shallow subsoil, firstly as separate indicators of hazard status, and then as combined factors.

The main outcomes can be summarized as follows:

- The use of the AHP approach allowed the authors to prioritize indicators by using different weights provided by pairwise comparisons and to verify the consistency. Nevertheless, a certain degree of subjectivity remains, which is intrinsic in the classification and weighting.
- The combined hazard map of freshwater–saltwater interface depth and average electrical resistivity allowed the authors to capture the salinization threat on the agricultural zone without neglecting that on the underlying shallow subsoil. The vulnerability maps that were obtained by considering the two hazard statuses separately depict a less realistic representation of the fragilities of the farmland system, while their combination adjusts some classes apparently over-/underestimated.
- The vulnerability of Venice farmland system is in the strong and extreme classes in about 30% of the area, marginal and moderate in the 28%, and negligible in the 40%.
- The outcomes of this research, compared with the previous assessments, confirm the heterogeneous distribution of the vulnerability in the study area. However, the differences between the two maps should be cautiously interpreted, because they focus on different targets, characterization of the sensitivity of the farmland system, and conceptualization of the hazard status.

Although this study represents a step forward in understanding the Venice farmland's vulnerability to saltwater intrusion, the authors are aware that a number of uncertainties still need to be resolved by further studies, especially to address optimal strategies for mitigation and water-management plans. Therefore, the authors claim the need to account for further indicators to better describe the sensitivity of the farmland system, such as the variability of the precipitation, details on the agricultural type cover, and the physiology of crops. In addition, the authors raise the issue of defining fixed rules both in the vulnerability assessment approach and in the choice of indicators acting to facilitate comparisons among different case studies.

References

1. Poulter, B.; Goodall, J.L.; Halpin, P.N. Applications of network analysis for adaptive management of artificial drainage systems in landscapes vulnerable to sea level rise. *J. Hydrol.* **2008**, *357*, 207–217. [CrossRef]
2. Rasmussen, P.; Sonnenborg, T.O.; Goncear, G.; Hinsby, K. Assessing impacts of climate change, sea level rise, and drainage canals on saltwater intrusion to coastal aquifer. *Hydrol. Earth Syst. Sci.* **2013**, *17*, 421–443. [CrossRef]
3. Tully, K.L.; Weissman, D.; Wyner, W.J.; Miller, J. Soils in transition: Saltwater intrusion alters soil chemistry in agricultural fields. *Biogeochemistry* **2019**, *142*, 339–356. [CrossRef]
4. Maas, E.; Grattan, S.R. Crop Yields as Affected by Salinity. In *Agricultural drainage*; American Society of Agronomy, Inc.: Madison, WI, USA; Crop Science Society of America, Inc.: Madison, WI, USA; Soil Science Society of America, Inc.: Madison, WI, USA, 1999; pp. 55–108.
5. Mastrocicco, M.; Colombani, N. The issue of groundwater salinization in coastal areas of the mediterranean region: A review. *Water* **2021**, *13*, 90. [CrossRef]
6. Weis, S.W.M.; Agostini, V.N.; Roth, L.M.; Gilmer, B.; Schill, S.R.; Knowles, J.E.; Blyther, R. Assessing vulnerability: An integrated approach for mapping adaptive capacity, sensitivity, and exposure. *Clim. Change* **2016**, *136*, 615–629. [CrossRef]
7. Field, C.B.; Barros, V.R.; Dokken, D.J.; Mach, K.J.; Mastrandrea, M.D.; Bilir, T.E.; Chatterjee, M.; Ebi, K.L.; Estrada, Y.O.; Genova, R.C.; et al. (Eds.) *IPCC Climate Change 2014. Impacts, Adaptation, and Vulnerability. Part A: Global and Sectoral Aspects. Contribution of Working Group II to the Fifth Assessment Report of the Intergovernmental Panel on Climate Change*; Cambridge University Press: Cambridge, UK, 2014; ISBN 9781107641655.
8. Field, C.B.; Barros, V.; Stocker, T.F.; Qin, D.; Dokken, D.J.; Ebi, K.L.; Mastrandrea, M.D.; Mach, K.J.; Plattner, G.-K.; Allen, S.K.; et al. (Eds.) *IPCC Managing the Risks of Extreme Events and Disasters to Advance Climate Change Adaptation. A Special Report of Working Groups I and II of the Intergovernmental Panel on Climate Change*; Cambridge University Press: Cambridge, UK, 2012; ISBN 9781139177245.
9. Fussel, H.-M.; Klein, R.J.T. Climate change vulnerability assessments: An evolution of conceptual thinking. *Clim. Change* **2006**, *75*, 301–329. [CrossRef]
10. Parizi, E.; Mossa, S.; Ataie-ashtiani, B.; Simmons, C.T. Vulnerability mapping of coastal aquifers to seawater intrusion: Review, development and application. *J. Hydrol.* **2019**, *570*, 555–573. [CrossRef]
11. Goyal, D.; Haritash, A.K.; Singh, S.K. A comprehensive review of groundwater vulnerability assessment using index-based, modelling and coupling methods. *J. Environ. Manag.* **2021**, *296*, 113161. [CrossRef]
12. Lobo-Ferreira, J.P.; Chachadi, A.G.; Diamantino, C.; Henriques, M.J. Assessing aquifer vulnerability to seawater intrusion using GALDIT method: Part 1—Application to the Portuguese Aquifer of Monte Gordo. In Proceedings of the Fourth Inter-Celtic Colloquium on Hydrology and Management of Water Resources, Guimarães, Portugal, 11–13 July 2005; International Association of Hydrological Sciences: Wallingford, UK, 2005; pp. 161–171.
13. Chachadi, A.G.; Lobo-Ferreira, J.P. Sea water intrusion vulnerability mapping of aquifers using the GALDIT method. *COASTIN A Coast. Policy Res. Newsl.* **2001**, *4*, 7–9.
14. Chachadi, A.G.; Lobo-Ferreira, J.P. Assessing aquifer vulnerability to sea-water intrusion using GALDIT method: Part 2—GALDIT Indicators Description. In Proceedings of the Fourth Inter-Celtic Colloquium on Hydrology and Management of Water Resources, Guimarães, Portugal, 11–13 July 2005; International Association of Hydrological Sciences: Wallingford, UK, 2005; pp. 172–180.
15. Bordbar, M.; Neshat, A.; Javadi, S.; Pradhan, B.; Aghamohammadi, H. Meta-heuristic algorithms in optimizing GALDIT framework: A comparative study for coastal aquifer vulnerability assessment. *J. Hydrol.* **2020**, *585*, 124768. [CrossRef]
16. Kazakis, N.; Busico, G.; Colombani, N.; Mastrocicco, M.; Pavlou, A.; Voudouris, K. GALDIT-SUSI a modified method to account for surface water bodies in the assessment of aquifer vulnerability to seawater intrusion. *J. Environ. Manage.* **2019**, *235*, 257–265. [CrossRef] [PubMed]
17. Trabelsi, N.; Triki, I.; Hentati, I.; Zairi, M. Aquifer vulnerability and seawater intrusion risk using GALDIT, GQISWI and GIS: Case of a coastal aquifer in Tunisia. *Environ. Earth Sci.* **2016**, *75*, 669. [CrossRef]
18. Recinos, N.; Kallioras, A.; Pliakas, F.; Schuth, C. Application of GALDIT index to assess the intrinsic vulnerability to seawater intrusion of coastal granular aquifers. *Environ. Earth Sci.* **2015**, *73*, 1017–1032. [CrossRef]
19. Busico, G.; Buffardi, C.; Ntona, M.M.; Vigliotti, M.; Colombani, N.; Mastrocicco, M.; Ruberti, D. Actual and forecasted vulnerability assessment to seawater intrusion via GALDIT-SUSI in the Volturno river mouth (Italy). *Remote Sens.* **2021**, *13*, 3632. [CrossRef]
20. Bordbar, M.; Neshat, A.; Javadi, S. A new hybrid framework for optimization and modification of groundwater vulnerability in coastal aquifer. *Environ. Sci. Pollut. Res.* **2019**, *26*, 21808–21827. [CrossRef] [PubMed]
21. Nasri, G.; Hajji, S.; Aydi, W.; Boughariou, E.; Allouche, N.; Bouri, S. Water vulnerability of coastal aquifers using AHP and parametric models: Methodological overview and a case study assessment. *Arab. J. Geosci.* **2021**, *14*, 59. [CrossRef]
22. Gorgij, A.D.; Moghaddam, A.A. Vulnerability Assessment of saltwater intrusion using simplified GAPDIT method: A case study of Azarshahr Plain Aquifer, East Azerbaijan, Iran. *Arab. J. Geosci.* **2016**, *9*, 106. [CrossRef]
23. Saaty, T.L. How to make a decision: The analytic hierarchy process. *Eur. J. Oper. Res.* **1990**, *48*, 9–26. [CrossRef]
24. Kazakis, N. Delineation of suitable zones for the application of Managed Aquifer Recharge (MAR) in coastal aquifers using quantitative parameters and the analytical hierarchy process. *Water* **2018**, *10*, 804. [CrossRef]
25. Nguyen, T.D.L.; Bleys, B. Applying analytic hierarchy process to adaptation to saltwater intrusion in Vietnam. *Sustainability* **2021**, *13*, 2311. [CrossRef]

26. Gambolati, G.; Putti, M.; Teatini, P.; Camporese, M.; Ferraris, S.; Gasparetto Stori, G.; Nicoletti, V.; Silvestri, S.; Rizzetto, F.; Tosi, L. Peat land oxidation enhances subsidence in the venice watershed. *EOS* **2005**, *86*, 217–224. [CrossRef]

27. Carbognin, L.; Gambolati, G.; Putti, M.; Rizzetto, F.; Teatini, P. Soil contamination and land subsidence raise concern in the Venice watershed, Italy. *WIT Trans. Ecol. Environ.* **2006**, *99*, 691–700. [CrossRef]

28. Carbognin, L.; Tosi, L. *Il Progetto Ises per L'Analisi dei Processi di Intrusione Salina e Subsidenza nei Territori Meridionali delle Provincie di Padova e Venezia*; Istituto per lo Studio della Dinamica delle Grandi Masse: Venezia, Italy, 2003.

29. Da Lio, C.; Carol, E.; Kruse, E.; Teatini, P.; Tosi, L. Saltwater contamination in the managed low-lying farmland of the Venice coast, Italy: An assessment of vulnerability. *Sci. Total Environ.* **2015**, *533*, 356–369. [CrossRef]

30. Tosi, L.; Da Lio, C.; Teatini, P.; Menghini, A.; Viezzoli, A. Continental and marine surficial water - Groundwater interactions: The case of the southern coastland of Venice (Italy). *Proc. Int. Assoc. Hydrol. Sci.* **2018**, *379*, 387–392. [CrossRef]

31. Lovrinović, I.; Bergamasco, A.; Srzić, V.; Cavallina, C.; Holjević, D.; Donnici, S.; Erceg, J.; Zaggia, L.; Tosi, L. Groundwater monitoring systems to understand sea water intrusion dynamics in the Mediterranean: The Neretva valley and the southern Venice coastal aquifers case studies. *Water* **2021**, *13*, 561. [CrossRef]

32. Tiozzo, P.G. *Lo Stabilimento Jappelli-Testa e la Bonifica Dell'Ultimo Lembo del Foresto in Chioggia e il Suo Territorio*; Ministero dell'Agricoltura, Bonifica e Programmazione nel Veneto: Venice, Italy, 1974.

33. Zecchin, M.; Brancolini, G.; Tosi, L.; Rizzetto, F.; Caffau, M.; Baradello, L. Anatomy of the Holocene succession of the southern Venice lagoon revealed by very high-resolution seismic data. *Cont. Shelf Res.* **2009**, *29*, 1343–1359. [CrossRef]

34. Tosi, L.; Teatini, P.; Brancolini, G.; Zecchin, M.; Carbognin, L.; Affatato, A.; Baradello, L. Three-dimensional analysis of the Plio-Pleistocene seismic sequences in the Venice Lagoon (Italy). *J. Geol. Soc.* **2012**, *169*, 507–510. [CrossRef]

35. Donnici, S.; Serandrei-Barbero, R.; Canali, G. Evidence of climatic changes in the Venetian Coastal Plain (Northern Italy) during the last 40,000 years. *Sediment. Geol.* **2012**, *281*, 139–150. [CrossRef]

36. Canali, G.; Capraro, L.; Donnici, S.; Rizzetto, F.; Serandrei-Barbero, R.; Tosi, L. Vegetational and environmental changes in the eastern Venetian coastal plain (Northern Italy) over the past 80,000 years. *Palaeogeogr. Palaeoclimatol. Palaeoecol.* **2007**, *253*, 300–316. [CrossRef]

37. Storms, J.E.A.; Weltje, G.J.; Terra, G.J.; Cattaneo, A.; Trincardi, F. Coastal dynamics under conditions of rapid sea-level rise: Late Pleistocene to Early Holocene evolution of barrier–lagoon systems on the northern Adriatic shelf (Italy). *Quat. Sci. Rev.* **2008**, *27*, 1107–1123. [CrossRef]

38. Zecchin, M.; Caffau, M.; Tosi, L. Relationship between peat bed formation and climate changes during the last glacial in the Venice area. *Sediment. Geol.* **2011**, *238*, 172–180. [CrossRef]

39. Donnici, S.; Serandrei-Barbero, R.; Bini, C.; Bonardi, M.; Lezziero, A. The caranto paleosol and its role in the early urbanization of Venice. *Geoarchaeology* **2011**, *26*, 514–543. [CrossRef]

40. Tosi, L.; Rizzetto, F.; Bonardi, M.; Donnici, S.; Serandrei-Barbero, R.; Toffoletto, F. *Note Illustrative della Carta Geologica d'Italia alla Scala 1:50.000. Foglio 128, Venezia*; Servizio Geologico d'Italia: Rome, Italy, 2007.

41. Tosi, L.; Rizzetto, F.; Bonardi, M.; Donnici, S.; Serandrei-Barbero, R.; Toffoletto, F. *Note Illustrative della Carta Geologica d'Italia alla Scala 1:50.000. Foglio 148-149, Chioggia-Malamocco*; Servizio Geologico d'Italia: Rome, Italy, 2007; 164.

42. Tosi, L.; Rizzetto, F.; Zecchin, M.; Brancolini, G.; Baradello, L. Morphostratigraphic framework of the Venice Lagoon (Italy) by very shallow water VHRS surveys: Evidence of radical changes triggered by human-induced river diversions. *Geophys. Res. Lett.* **2009**, *36*, 1–5. [CrossRef]

43. Gambolati, G.; Teatini, P. Numerical Analysis of Land Subsidence due to Natural Compaction of the Upper Adriatic Sea Basin. In *CENAS. Coastline Evolution of the Upper Adriatic Sea due to Sea Level Rise and Natural and Anthropogenic Land Subsidence*; Gambolati, G., Ed.; Springer: Dordrecht, The Netherlands, 1998; pp. 103–131.

44. Rizzetto, F.; Tosi, L.; Carbognin, L.; Bonardi, M.; Teatini, P. Geomorphic setting and related hydrogeological implications of the coastal plain south of the Venice Lagoon, Italy. In Proceedings of the Hydrology of Mediterranean and Semiarid Regions, Montpellier, France, 1–4 April 2003; International Association of Hydrological Sciences: Wallingford, UK; pp. 463–470.

45. Gambolati, G.; Putti, M.; Teatini, P.; Gasparetto Stori, G. Subsidence due to peat oxidation and impact on drainage infrastructures in a farmland catchment south of the Venice Lagoon. *Environ. Geol.* **2006**, *49*, 814–820. [CrossRef]

46. Fornasiero, A.; Gambolati, G.; Putti, M.; Teatini, P.; Ferraris, S.; Pitacco, A.; Rizzetto, F.; Tosi, L.; Bonardi, M.; Gatti, P. Subsidence due to peat soil loss in the Zennare basin (Italy): Design and set-up of the field experiment. In *Scientific Research and Safeguarding of Venice*; Campostrini, P., Ed.; Istituto Veneto di Scienze Lettere ed Arti: Venice, Italy, 2002; pp. 201–215.

47. Camporese, M.; Putti, M.; Salandin, P.; Teatini, P. Spatial variability of CO2 efflux in a drained cropped peatland south of Venice, Italy. *J. Geophys. Res. Biogeosciences* **2008**, *113*, G04018. [CrossRef]

48. Tosi, L.; Carbognin, L.; Teatini, P.; Rosselli, R.; Gasparetto Stori, G. The ISES Project subsidence monitoring of the catchment basin south of the Venice Lagoon (Italy). In *Land subsidence: Proceedings of the Sixth International Symposium on Land Subsidence, Ravenna, Italy, 24–29 September 2000*; CNR, Grupo Nazionale per la Difesa dalle Catastrofi Idrogeologiche: Venice, Italy, 2000; Volume 2, pp. 113–126.

49. Zechner, E.; Konz, M.; Younes, A.; Huggenberger, P. Effects of tectonic structures, salt solution mining, and density-driven groundwater hydraulics on evaporite dissolution (Switzerland). *Hydrogeol. J.* **2011**, *19*, 1323–1334. [CrossRef]

50. De Franco, R.; Biella, G.; Tosi, L.; Teatini, P.; Lozej, A.; Chiozzotto, B.; Giada, M.; Rizzetto, F.; Claude, C.; Mayer, A.; et al. Monitoring the saltwater intrusion by time lapse electrical resistivity tomography: The Chioggia test site (Venice Lagoon, Italy). *J. Appl. Geophys.* **2009**, *69*, 117–130. [CrossRef]

51. Viezzoli, A.; Tosi, L.; Teatini, P.; Silvestri, S. Surface water-groundwater exchange in transitional coastal environments by airborne electromagnetics: The Venice Lagoon example. *Geophys. Res. Lett.* **2010**, *37*, L01402. [CrossRef]

52. Teatini, P.; Tosi, L.; Viezzoli, A.; Baradello, L.; Zecchin, M.; Silvestri, S. Understanding the hydrogeology of the Venice Lagoon subsurface with airborne electromagnetics. *J. Hydrol.* **2011**, *411*, 342–354. [CrossRef]

53. Morari, F.; Meggio, F.; Lunardon, A.; Scudiero, E.; Forestan, C.; Farinati, S.; Varotto, S. Time course of biochemical, physiological, and molecular responses to field-mimicked conditions of drought, salinity, and recovery in two maize lines. *Front. Plant Sci.* **2015**, *6*, 314. [CrossRef]

54. Tosi, L.; Da Lio, C.; Donnici, S.; Strozzi, T.; Teatini, P. Vulnerability of Venice's coastland to relative sea-level rise. *Proc. Int. Assoc. Hydrol. Sci.* **2020**, *382*, 689–695. [CrossRef]

55. Zanchettin, D.; Bruni, S.; Raicich, F.; Lionello, P.; Adloff, F.; Androsov, A.; Antonioli, F.; Artale, V.; Carminati, E.; Ferrarin, C.; et al. Sea-level rise in Venice: Historic and future trends (review article). *Nat. Hazards Earth Syst. Sci.* **2021**, *21*, 2643–2678. [CrossRef]

56. Bondesan, A.; Primon, S.; Bassan, V.; Vitturi, A. *Carta delle Unità Geologiche della Provincia di Venezia*; Cierre: Verona, Italy, 2008.

57. Da Lio, C.; Tosi, L.; Zambon, G.; Vianello, A.; Baldin, G.; Lorenzetti, G.; Manfè, G.; Teatini, P. Long-term groundwater dynamics in the coastal confined aquifers of Venice (Italy). *Estuar. Coast. Shelf Sci.* **2013**, *135*, 248–259. [CrossRef]

58. ARPAV Valutazione della permeabilità e del gruppo idrologico dei suoli del Veneto; 2011. Available online: https://www.arpa.veneto.it/temi-ambientali/suolo/file-e-allegati/documenti/minacce-didegradazione/Relazione_permeabilita_Gruppo_Idrologico_giu2011_def.pdf (accessed on 23 December 2021).

59. Vitturi, A.; Bassan, V.; Mazzuccato, A.; Primon, S.; Bondesan, A.; Ronchese, F.; Zangheri, P. *Atlante Geologico della Provincia di Venezia. Note Illustrative*; Provincia di Venezia: Venice, Italy, 2011.

60. USDA Hydrologic Soil Groups. *National Engineering Handbook*; U.S. Department of Agriculture, Natural Resources Conservation Service: Washington, DC, USA, 2009; p. 13.

61. Cressie, N. The origins of kriging. *Math. Geol.* **1990**, *22*, 239–252. [CrossRef]

62. Saaty, T.L. Decision-making with the AHP: Why is the principal eigenvector necessary. *Eur. J. Oper. Res.* **2003**, *145*, 85–91. [CrossRef]

63. Cho, F. Analytic Hierarchy Process for Survey Data in R. Vignettes for the ahpsurvey package (ver 0.4.1). 2019. Available online: https://cran.r-project.org/web/packages/ahpsurvey/vignettes/my-vignette.html (accessed on 23 December 2021).

64. Azizi, F.; Vadiati, M.; Asghari, A.; Amirhossein, M.; Jan, N. A hydrogeological-based multi-criteria method for assessing the vulnerability of coastal aquifers to saltwater intrusion. *Environ. Earth Sci.* **2019**, *78*, 548. [CrossRef]

65. Gattacceca, J.C.; Vallet-Coulomb, C.; Mayer, A.; Claude, C.; Radakovitch, O.; Conchetto, E.; Hamelin, B. Isotopic and geochemical characterization of salinization in the shallow aquifers of a reclaimed subsiding zone: The southern Venice Lagoon coastland. *J. Hydrol.* **2009**, *378*, 46–61. [CrossRef]

66. Thywissen, K. *Components of Risk: A Comparative Glossary*; United Nations University, Institute of Environment and Human Security: Bonn, Germany, 2006; ISBN 3981058208.

67. Manyena, S.B. The concept of resilience revisited. *Disasters* **2006**, *30*, 433–450. [CrossRef]